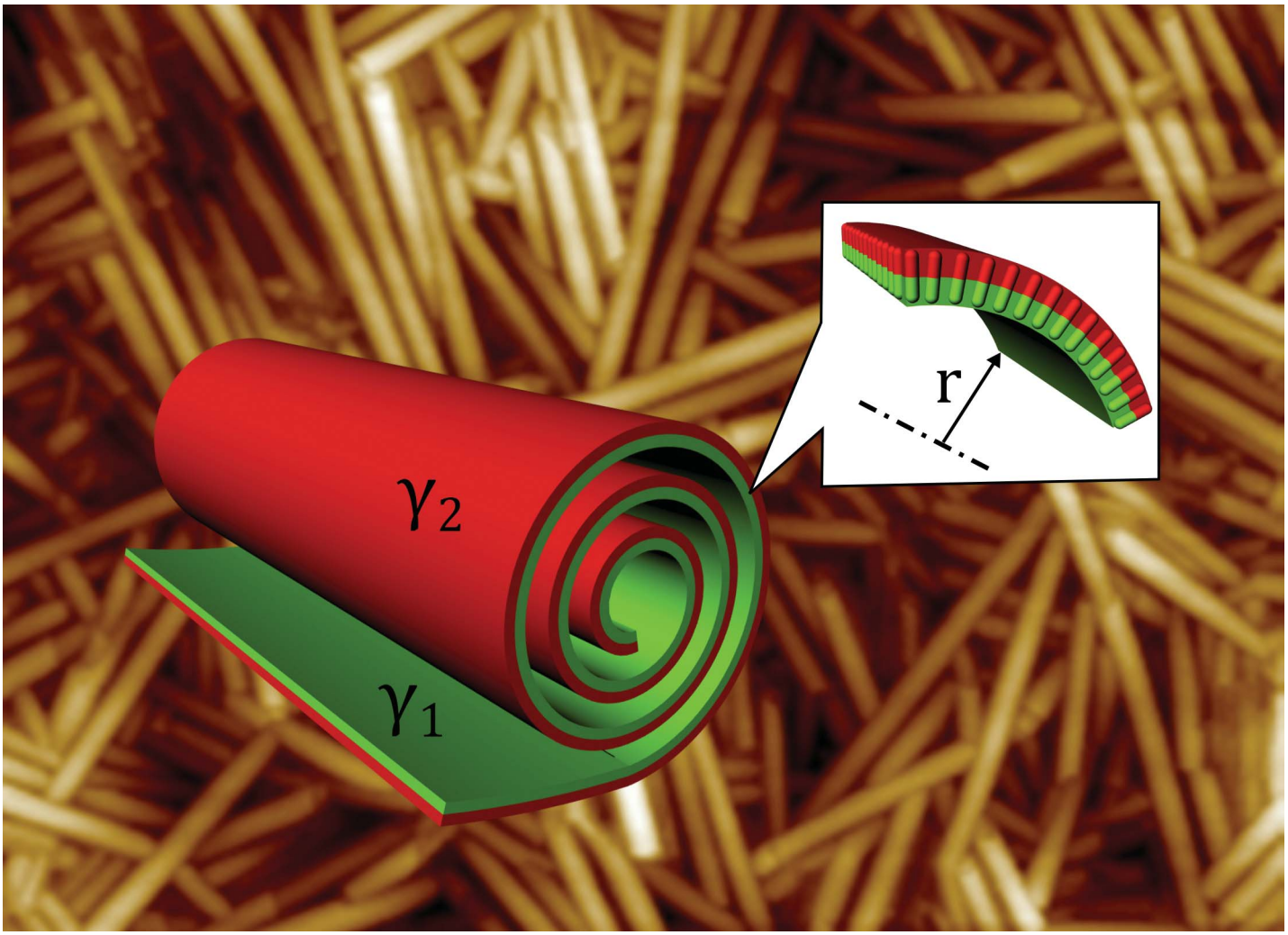


**Showcasing research from the Institute of Physics of the Czech Academy of Sciences in Prague, in collaboration with the Faculty of Chemistry, University of Warsaw.**

Organic nanotubes created from mesogenic derivatives

We present a facile route to prepare nanotubes from rod-like mesogens dissolved in typical organic solvents. For selected types of chiral rod-like molecules, both enantiomers, as well as the racemic mixtures, formed nanotubes *via* slow evaporation from solution, regardless of the solvent, concentration, or deposition surface. The obtained supramolecular assemblies were studied using AFM, TEM, and SEM microscopy techniques, IR, UV-Vis spectroscopy, and x-ray diffraction.

## As featured in:


See Vladimíra Novotná *et al.*, *Nanoscale Adv.*, 2019, **1**, 2835.

ROYAL SOCIETY OF CHEMISTRY | Celebrating IYPT 2019

rsc.li/nanoscale-advances

Registered charity number: 207890

Nanoscale Advances



COMMUNICATION

View Article Online
View Journal | View Issue



Cite this: *Nanoscale Adv.*, 2019, **1**, 2835

# Organic nanotubes created from mesogenic derivatives†

Vladimíra Novotná, *[a] Věra Hamplová,[a] Lubor Lejček,[a] Damian Pociecha,[b] Martin Cigl,[a] Ladislav Fekete,[a] Milada Glogarová,[a] Lucie Bednárová,[c] Pawel W. Majewski[b] and Ewa Gorecka[b]

Received 21st March 2019
Accepted 15th June 2019

DOI: 10.1039/c9na00175a

rsc.li/nanoscale-advances

A facile route to prepare nanotubes from rod-like mesogens dissolved in typical organic solvents is reported. For selected types of chiral rod-like molecules, nanotubes were formed from both enantiomers and racemic mixtures by slow evaporation from solution, regardless of the solvent, concentration or deposition type. The obtained supramolecular assemblies were studied using AFM, TEM and SEM techniques, and other experimental techniques (IR, UV-Vis spectroscopy and X-ray diffraction) were also applied. The difference in the surface tension at opposite crystallite surfaces is suggested as a possible mechanism for nanotube nucleation. We propose a quite new rolling-up mechanism related to the surface tension difference at opposite crystallite surfaces.



Nanotubular morphology can be observed for various materials. The most studied examples are carbon nanotubes (CNTs) formed by rolling up graphite sheets around the edges.[1] Since the discovery of CNTs,[2] other types of layered inorganic nanotubes have been described, *e.g.* $WS_2$, $MoS_2$ or $TiO_2$ metal chalcogenide nanotubes.[3,4] Likewise, nanotubes can be formed from organic molecules and macromolecules; organic nanotubes (ONTs) are of great interest and represent a challenging topic in the area of materials chemistry. Various types of ONTs have been synthesized and their applications have been actively explored in recent years.[5] They offer potential applications as electronically and biologically active materials because of their better biodegradability and biocompatibility in comparison with inorganic materials with covalent linkages.[6] In addition, the surfaces, morphologies, sizes, and functionalities of ONTs can be easily tuned by modification of the nanotube-forming molecules or the self-assembly process. The utilization of the inner channel of the nanotubes has also attracted much attention as it offers potential for filtration applications[7] and a possibility to capture and release various guest molecules in a controllable way.[8,9]

Organic nanotubes spontaneously self-assemble through various molecular interactions such as a hydrogen bonding, van der Waals forces and π–π stacking; molecular shape and other conditions play a role as well.[5] As a driving force for the scrolling of flat sheets into nanotubes, the chirality of the materials or the layer curvature,[10] or the polarization charges at the opposite sides of the sheet were suggested.[3] Reducing the surface energy of a flat sheet in solution is also a possible scrolling mechanism that leads to the formation of ONTs.[5] The largest group of materials forming ONTs comprises amphiphilic molecules possessing hydrophilic and hydrophobic parts and a few reviews have been published recently.[10,11] In most cases lipid nanotubes involve helically coiled ribbon structures.[12,13] The nanotubes derived from terphenylene-diamides have been proved to exhibit a scroll-type structure formed by the rolled-up sheets.[14] Only rarely ONTs are built from molecules with no or small asymmetry in the molecular structure.[15]

Liquid crystalline (LC) phases are formed by the self-assembly of organic molecules; the most commonly observed ones are mesophases with lamellar morphology (smectics). In rare cases, the morphology of such phases is more complex than just flat layers *e.g.* nano-ribbons or sponge type structures can be formed.[3a,16,17] So far, the formation of nanotubes from mesogenic compounds has been reported only for bent-core molecules exhibiting a B4 phase.[18]

Herein, we present a new type of mesogenic rod-like compounds, which spontaneously form nanotubes in the crystalline state. The studied chiral rod-like molecules are in the crystalline state at room temperature and exhibit a sequence of liquid crystalline phases above the melting point.[19] The rolled-up nanotubes are created from solution during solvent evaporation. The nanotube formation process was studied as a function of the

[a]*Institute of Physics of the Czech Academy of Sciences, Na Slovance 2, CZ-182 21 Prague 8, Czech Republic. E-mail: novotna@fzu.cz; Fax: +420286890527; Tel: +420266053111*

[b]*Faculty of Chemistry, University of Warsaw, ul. Zwirki i Wigury 101, 02-089 Warsaw, Poland. E-mail: gorecka@chem.uw.edu.pl; Tel: +48228221075*

[c]*Institute of Organic Chemistry and Biochemistry of the CAS, Flemingovo n. 2,166 10 Prague 6, CZ-182 21 Prague 6, Czech Republic*

† Electronic supplementary information (ESI) available. See DOI: 10.1039/c9na00175a

molecular structure and type of the solvent. We used atomic force microscopy (AFM) and electron microscopy (SEM) to study the morphology of the nano-assemblies. Infrared and UV spectroscopy and X-ray measurements provided additional information about the self-assembly behaviour at the molecular level.

Chemical formulas of the studied compounds, denoted as 10ZBBL, 10ZBDL and *m*ZBL, are shown in Fig. 1. Materials *m*ZBL have been prepared by a synthetic route described previously.[19] Both chiral centers for *m*ZBL compounds are of *S* type, so we denote them as *m*ZBL(*S*,*S*). The details of 10ZBBL and 10ZBDL synthesis are given in the ESI.† Compounds 10ZBBL and 10ZBDL have been synthesized in both enantiomeric forms and as a racemic mixtures. At room temperature, all studied compounds are crystalline and melt to the LC smectic phase at about 65 °C. The mesomorphic properties of *m*ZBL were studied previously, and the compound exhibited an unusual sequence of smectic phases.[19]

The nanotubes were prepared at room temperature, the molecules were dissolved in an organic solvent and the solution was spread on a solid surface; the subsequent slow spontaneous evaporation of the solvent yielded thin films. The morphology of the films has been studied using AFM and SEM techniques. The methods (AFM, SEM, IR and UV-vis spectroscopy and X-ray diffraction) and equipment used in this study are described in detail in the ESI.†

Nanotube growth was studied in detail under different conditions for 10ZBBL and *m*ZBL materials (see Fig. 1). We tested several types of organic polar or non-polar solvents, in which the compounds are soluble: cyclohexane, toluene and acetone at various concentrations: $10^{-3}$ to $10^{-2}$ mol $l^{-1}$. Also, the influence of the solvent evaporation rate was verified. Additionally, the nanotubes were prepared on several types of solid surfaces, such as glass, KBr, sapphire and lithium niobate ($LiNbO_3$), and it was established that nanotube growth from the solution does not depend on the type of the substrate. For 10ZBBL(*S*), 10ZBBL(*R*) and *m*ZBL(*S*,*S*) materials the shape and size of the obtained nanotubes were very similar. No differences were found while using pure enantiomers or racemic mixtures of 10ZBBL; thus we can exclude the optical purity of the compound as a necessary condition for nanotube growth. The AFM images revealed that the nanotube diameter is 50 to 60 nm with an inner channel diameter of ~20 nm (Fig. 2), regardless of the film preparation conditions. On the other hand, the length of the nanotubes varied from sample to sample. Close inspection of the nanotube surface evidenced

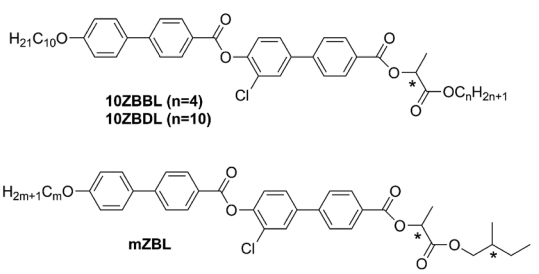


Fig. 1 Chemical formula of 10ZBBL, 10ZBDL and *m*ZBL compounds.

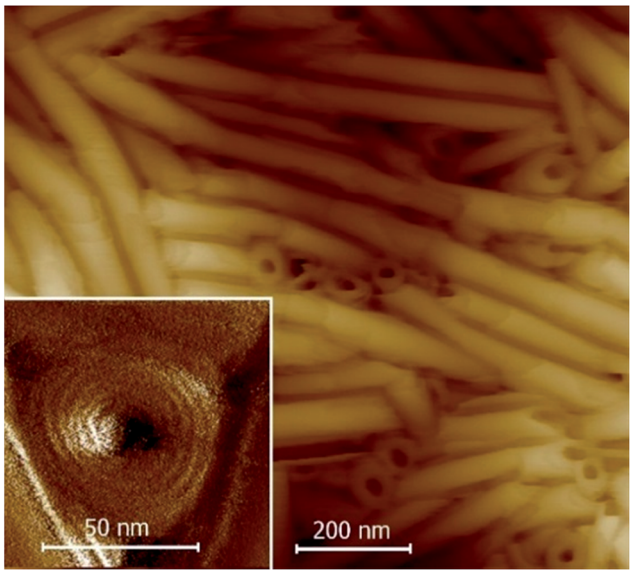


Fig. 2 AFM images of the 10ZBL(*S*,*S*) film grown by evaporation from acetone solution. In the inset, the enlarged view of a nanotube oriented perpendicular to the surface is shown.

the roll-up mechanism of their formation. The thickness of the nanotube wall is ~15 nm and small 3–5 nm steps are visible. Thus the nanotube wall comprises several mono-molecular layers wound one over the other. Apart from the typical organic solvents, we have also tested a chiral solvent (*S*)-(2-methylbutyl)methylether (see the ESI† for more information) and confirmed the presence of nanotubes for both pure enantiomers and racemic mixtures of 10ZBBL, and no chiral discrimination effects were observed.

The AFM images showed that majority of the nanotubes grow parallel to the surface (Fig. 2 and 3); only in few images were we able to detect nanotubes oriented with their axes perpendicular

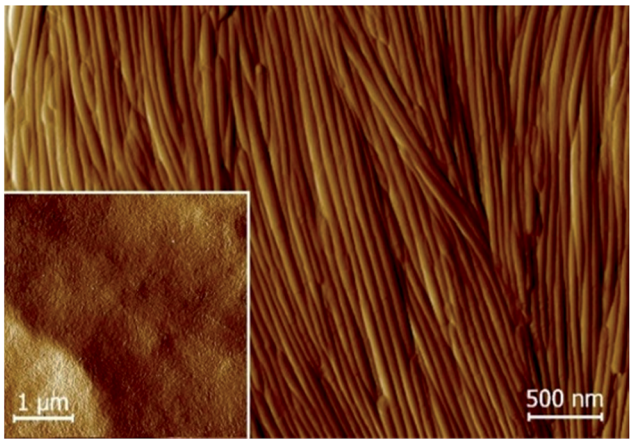


Fig. 3 AFM image of the 10ZBLL(*S*) film on a $LiNbO_3$ substrate showing parallel alignment of the nanotubes over a large area. In the inset, the AFM image of the crystalline phase of 10ZBBL(rac) obtained for a sample recrystallized from the smectic phase a smooth surface with no complex morphology is shown.

to the surface (inset in Fig. 2 and S3 in the ESI†). Moreover, in numerous experiments, the tubes were found mutually parallel to each other over large areas (Fig. 3). Under a weak shearing between glass plates or polymer foils we were able to orient the nanotubes in macroscopic areas, with their axes parallel to the shearing direction, which was proven by X-ray diffraction studies (Fig. 5). The high quality of the alignment was tested by performing X-ray diffraction in different sample areas.

We have characterized nanotubes by SEM and TEM techniques. For SEM, the film was sputtered with a metallic layer (see Fig. 4). The TEM images of pure organic materials were not convincing enough. We mixed the studied compounds with silver nanoparticles, which provided a better contrast, and we confirmed the hollow character of the nanotubes. TEM images are shown in the inset of Fig. 4 and in the ESI (Fig. S9†).

X-ray studies confirmed the crystalline character of the nanotubes (Fig. 5); the large width of the recorded X-ray diffraction signals was a result of the highly limited size of the diffracting objects.[20] The material crystallized in an orthorhombic unit cell (for 9ZBL(*S*,*S*) the crystallographic unit cell parameters are $a = 42$ Å, $b = 15$ Å and $c = 4.5$ Å). The crystal had a lamellar structure with a layer spacing ($a$ crystallographic parameter) similar to that found in the smectic phase and which corresponded to the molecular length. The orientation of the signals in the XRD patterns for the sample aligned by shearing suggested that the nanotube axis was oriented along the $b$ crystallographic unit cell direction. The nanotubes melted at the transition from the crystalline to liquid crystalline phase (SmC). On cooling back, the material recrystallized in the same crystalline form as found for ONTs (Fig. 5), but neither nanotubes nor any other supramolecular morphology was observed (Fig. 3 inset); apparently the presence of the solvent is crucial for nanotube formation.

The ONTs on the KBr substrate were studied using IR spectroscopy from room temperature until the material melted to the smectic phase and the spectra (3600–600 $cm^{-1}$) are presented in the ESI (Fig. S10–S12†). The main difference between the ONTs and the liquid crystalline phase was found in the C–H stretching spectral region (3000–2800 $cm^{-1}$). The spectral shift

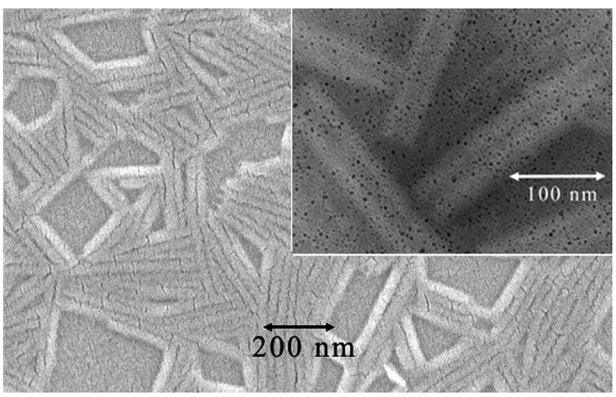


Fig. 4 SEM image taken for the 9ZBL(*S*,*S*) film, which was prepared from toluene solution. The surface was sputtered with a Ag layer. In the inset, the TEM image for 9ZBL(*S*,*S*) with Ag nanoparticles admixed for better contrast is shown.

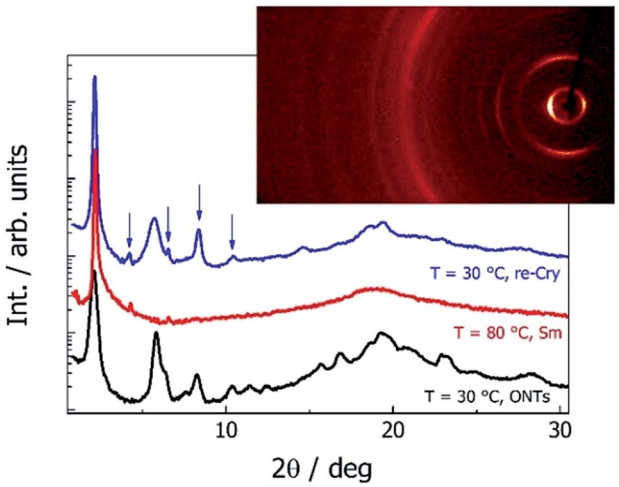


Fig. 5 X-ray diffraction patterns of compound 9ZBL(*S*,*S*): the nanotubes obtained from the toluene (black line) and smectic phase at $T = 80$ °C (red line) and the crystal formed from the melt (blue line). Arrows indicate harmonics of the main signal related to the layer thickness. In the inset, the 2D pattern obtained for ONTs is shown.

of the absorption maxima from 2922 $cm^{-1}$ to 2927 $cm^{-1}$ and 2852 $cm^{-1}$ to 2856 $cm^{-1}$ assigned to $\nu_A$(C–H) and $\nu_S$(C–H) of $CH_2$ groups, respectively, shows that the aliphatic chains liquidise at the transition to the liquid crystalline state.[21] The spectral shifts were also observed for the absorption maxima related to the carbonyl groups, for ONTs at 1724 $cm^{-1}$ (ester group at a terminal phenyl ring), 1744 $cm^{-1}$ (ester group between biphenyl units) and 1752 $cm^{-1}$ (ester group in the chiral tail). In the smectic phase the first two moved to 1726 $cm^{-1}$ and 1739 $cm^{-1}$, respectively, with comparable intensity to that at room temperature. The intensity of the band at 1752 $cm^{-1}$ decreases, probably corresponding to its degree of freedom,[22] and shifts to 1760 $cm^{-1}$. In the crystalline state of the ONTs, the violation of co-planar arrangement of the carbonyl group in the mesogenic core with the phenyl rings it is not excluded considering the spectral change of carbonyl and spectral shift and intensity change of the band at 1602 $cm^{-1}$, which is assigned to phenyl ring vibration. The creation of nanotubes causes the shift in the absorption maxima in the UV-vis spectral range towards a shorter wavelength in comparison to its reference position for the non-interacting molecules in solution (Fig. S13†). Such a hypsochromic shift indicates the presence of H-aggregates in the crystalline structure with a parallel orientation of the neighbouring molecules.

We have also analysed the films prepared from the 10ZBDL compound having a longer chiral alkyl chain ($n = 10$) than the 10ZBBL compound ($n = 4$) and did not observe the formation of nanotubes. The AFM images for 10ZBDL showed only flat 3–4 nm thick crystal plates (Fig. S5†). Moreover, among the homologues $m$ZBL(*S*,*S*) with various lengths of the non-chiral alkyl chain[19] ($m$ = 5–10), only compounds $m = 8$, 9 and 10 were found to form nanotubes. This clearly indicates a very delicate balance of forces responsible for nanotube creation with respect to the molecular structure.

The obtained results show that the mechanism responsible for the crystal layer curving and thus nucleation of the nanotubes is related to the crystal–solvent interactions that are different at opposite surfaces of the crystal layer. The broken up–down symmetry of the molecular orientation, which creates different surfaces of the crystal layer or/and the evaporation process itself and leads to different solvent concentrations at opposite crystal surfaces, might play an important role. Irrespective of the molecular packing in layers, the process of nanotube formation can be described using a phenomenological parameter – "surface tension". It is clear that the lack of balance in surface tension between two sides of a molecular layer becomes a driving force for the formation of a curved object, in the simplest case a rolled-up sheet. Let us determine the curvature radius, $r$, of a growing layer. The length of the layer arc of angle $\alpha$ is $r\alpha$. We suppose that the tangential force (per unit length in the direction parallel to the axis of layer rotation) on the inner surface, $-\partial(\gamma_1 r\alpha)/r\partial\alpha$, should be balanced by the tangential force on the outer surface, $-\partial(\gamma_2 r\alpha)/r\partial\alpha$, where $\gamma_1$ and $\gamma_2$ are the surface tensions of the inner and outer surfaces of a curved layer, respectively. The density of the elastic energy for the curved layer can be written[23] as:

$$f_{el} = \frac{K_1}{2}\left(\frac{1}{r_1}+\frac{1}{r_2}\right)^2 + \frac{K_2}{r_1 r_2}, \quad (1)$$

where $K_1$ and $K_2$ are the elastic constants and $r_1$ and $r_2$ are the principal radii of curvature of the layer. For cylinders, $r_1 = r$ and $r_2 = \infty$. The volume of the single crystal layer (per unit length) is $hr\alpha$, where $h$ is the layer thickness. Then, the tangential force due to the curvature of a layer (per unit length) will be given approximately by $-\partial\left(\frac{K_1}{2}\frac{h\alpha}{r}\right)\Big/ r\partial\alpha$. Finally, we obtain the force balance for a growing curved layer (per unit length along the rotation axis[24] (see Fig. 6)) in the form:

$$\gamma_1 = \gamma_2 + \frac{K_1 h}{2r^2} \quad (2)$$

The radius $r$ exists if $\gamma_2 < \gamma_1$ and for $\gamma_1 \to \gamma_2$ the radius increases. If $n$ layers are assembled together making a wall of thickness $nh$, then the energy of a nanotube (per unit length) can be rewritten as:

$$\pi K_1 \ln\frac{R}{r} + 2\pi(\gamma_1 r + \gamma_2 R). \quad (3)$$

We considered a cylinder with inner radius $r$ and outer radius $R = r + nh$. Observations show that the inner nanotube radius is typically about 10 nm. Assuming that the single crystal layer in a solvent has a similar bend elastic constant to a smectic liquid crystal, $K_1 \approx 10^{-11}$ J m$^{-1}$, for a layer of thickness $h \approx 3.5$ nm, we can estimate $\Delta\gamma = \gamma_1 - \gamma_2$ from eqn (3) as $\Delta\gamma \approx 1.75 \times 10^{-4}$ J m$^{-2}$, which is only ~1% of the surface tension of alkyl esters.[25] Such a difference of $\Delta\gamma$ can easily result from the broken up–down symmetry of the molecular orientation within the crystal layer or from the solvent concentration gradient across the sample thickness.

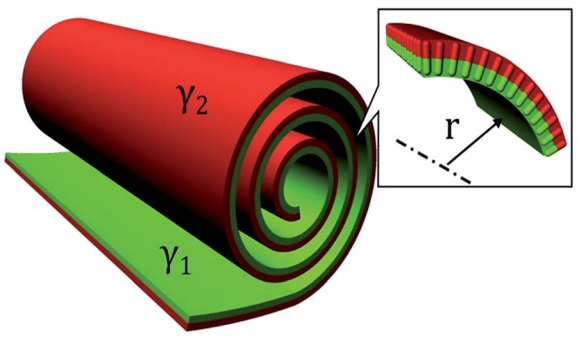


Fig. 6 Schematic of layers rolling up and ONT growth; coefficient $\gamma$ describes different surface tensions on the opposite side of the layer. In the inset, the molecular orientation is shown schematically.

## Conclusions

Let us point out that the character of the studied compounds is rather unusual for ONTs as the molecules are not amphiphilic, having alkyl chains at both molecular ends. The nanotubes' morphology is not influenced by the type of the organic solvent and the type of the substrate on which they are grown. Nanotubes formed from the 10ZBBL compound were observed for both *R* and *S* enantiomers as well as for the racemic mixture, in achiral and chiral solvents; therefore we can exclude the chiral discrimination effects for nanotube formation. On the other hand, the molecular end group modification easily leads to the loss of nanotube growth when the length of both terminal chains becomes similar. The molecules forming ONTs have different terminal parts and thus asymmetry of the inner and outer surface of ONTs exists. This supports the hypothesis that the main factor governing nanotube formation is the asymmetry in surface tension at opposite surfaces of the crystal layer, resulting from the broken up–down symmetry of the molecular arrangement within the crystal layer. In spite of the fact that we are not able to tune the size of nanotubes, we have succeeded in aligning the nanotubes in micron size areas by shearing.

## Conflicts of interest

There are no conflicts to declare.

## Acknowledgements

This research was supported by projects 18-14497S (the Czech Science Foundation), MEYS LO1409 Infrastructure SAFMAT LM2015088 and by the National Science Centre (Poland) under Grant No. 2015/19/P/ST5/03813 received from the European Union's Horizon 2020 research and innovation programme under the Marie Skłodowska-Curie grant agreement No. 665778.

## References

1 S. Amelinckx, D. Bernaerts, X. B. Zhang, G. Van Tendeloo and J. Van Landuyt, *Science*, 1995, **267**, 1334–1338.
2 S. Iijima, *Nature*, 1991, 35456–35458.

 

3 (*a*) G. Seifert, T. Kohler and R. Tenne, *J. Phys. Chem. B*, 2002, **106**, 2497–2501; (*b*) W. Helfrich, *J. Chem. Phys.*, 1986, **85**, 1085–1087.
4 B. D. Yao, Y. F. Chan, X. Y. Zhang, W. F. Zhang, Z. Y. Yang and N. Wang, *Appl. Phys. Lett.*, 2003, **82**, 281–283.
5 (*a*) N. Kameta, H. Minamikawa and M. Masuda, *Soft Matter*, 2011, **7**, 4539–4561; (*b*) D. Bong, T. D Clark, J. R. Granja and M. R. Gradiri, *Angew. Chem., Int. Ed.*, 2001, **40**, 988–1011; (*c*) N. Kameta, H. Minamikawa, M. Masuda, G. Mizunoc and T. Shimizu, *Soft Matter*, 2008, **4**, 1681–1687.
6 T. Shimizu, N. Kameta, W. Ding and M. Masuda, *Langmuir*, 2016, **32**(47), 12242–12264.
7 (*a*) S. Arias, F. Freire, E. Quinoa and R. Riguera, *Angew. Chem., Int. Ed.*, 2014, **53**, 13720–13724; (*b*) H. Liu, J. Xu, Y. Li and Y. Li, *Acc. Chem. Res.*, 2010, **43**, 1496–1508.
8 (*a*) N. Kameta, M. Masuda, H. Minamikawa, Y. Mishima, I. Yamashita and T. Shimizu, *Chem. Mater.*, 2007, **19**, 3553–3560; (*b*) M. A. Boles, M. Engel and D. V. Talapin, *Chem. Rev.*, 2016, **116**, 11220–11289.
9 (*a*) G. John, M. Mason, P. M. Ajayan and J. S. Dordick, *J. Am. Chem. Soc.*, 2004, **126**, 15012–15013; (*b*) S. Cui, H. Liu, L. Gan, Y. Li and D. Zhu, *Adv. Mater.*, 2008, **20**, 2918–2925.
10 (*a*) T. Shimizu, M. Masuda and H. Minamikawa, *Chem. Rev.*, 2005, **105**, 1401–1443; (*b*) C. C. Lee, C. G. Grenier, E. W. Meijer and A. P. H. J. Schenning, *Chem. Soc. Rev.*, 2009, **38**, 671–683.
11 (*a*) T. G. Barclay, K. Constantopoulos and J. Matisons, *Chem. Rev.*, 2014, **114**, 10217–10291; (*b*) L. Zhang, H. Li, C. Sik Ha, H. Suh and I. Kim, *Langmuir*, 2010, **26**, 17890–17895.
12 (*a*) S. Komura and O.-Y. Zhong-can, *Phys. Rev. Lett.*, 1998, **81**, 473–476; (*b*) Y. Zhou and T. Shimizu, *Chem. Mater.*, 2008, **20**, 625–633.
13 Y. Huang, B. Quan, Z. Wei, G. Liu and L. Sun, *J. Phys. Chem. C*, 2009, **113**, 3929–3933.
14 Y. Chen, B. Zhu, F. Zhang, Y. Han and Z. Bo, *Angew. Chem., Int. Ed.*, 2008, **47**, 6015–6018.
15 Y. Chen, F. Zhang, B. Zhu, Y. Han and Z. Bo, *Chem.–Asian J.*, 2011, **6**, 226–233.
16 C. C. Lee, C. G. Grenier, E. W. Meijer and A. P. H. J. Schenning, *Chem. Soc. Rev.*, 2009, **38**, 671–683.
17 (*a*) M. R. Ghadiri, J. R. Granja, R. A. Milligan, D. E. McRee and N. Hazanovich, *Nature*, 1993, **366**(6453), 324–327; (*b*) J. M. Schnur, *Nature*, 1993, **262**, 1669–1675.
18 (*a*) E. Gorecka, N. Vaupotič, A. Zep and D. Pociecha, *Angew. Chem., Int. Ed.*, 2016, **55**, 12238–12242; (*b*) V. K. Le, H. Takezoe and F. Araoka, *Adv. Mater.*, 2017, **29**, 1602737.
19 (*a*) V. Novotná, V. Hamplová, N. Podoliak, M. Kašpar, M. Glogarová, D. Pociecha and E. Gorecka, *J. Mater. Chem.*, 2011, **21**, 14807–14811; (*b*) V. Novotná, M. Glogarová, M. Kašpar, V. Hamplová, E. Gorecka, D. Pociecha and M. Cepic, *Phys. Rev. E: Stat. Phys., Plasmas, Fluids, Relat. Interdiscip. Top.*, 2011, **83**, 020701.
20 A. L. Patterson, *Phys. Rev.*, 1939, **56**, 978–982.
21 (*a*) R. Mendelsohn and D. J. Moore, *Chem. Phys. Lipids*, 1998, **96**, 141–157; (*b*) P. Wolfangel and K. Muller, *J. Phys. Chem. B*, 2003, **107**, 9918–9928.
22 N. Colthup, L. Daly and S. Wiberley, in *Introduction to infrared and Raman spectroscopy*, Elsevier, Academic Press, Boston, 3th edn, 1990, ch. 9, pp. 287–327.
23 P. Oswald and P. Pieranski, *Smectic and columnar liquid crystals*, Taylor and Francis, Boca Raton, 2006.
24 P.-G. deGennes, F. Brochard-Wyart and D. Quéré, *Capillarity and wetting phenomena: drops, bubbles, pearls, waves*, Springer Science + Business Media, New York, 2004.
25 K. M. Doll, B. R. Moser and S. Z. Erhan, *Energy Fuels*, 2007, **21**, 3044–3048.